Structure-Preserving Smoothing of Biomedical Images

Debora Gil[1], Aura Hernàndez-Sabaté[1], Mireia Brunat[2], Steven Jansen[3], and Jordi Martínez-Villalta[2]

[1] Computer Vision Center, Computer Science Department, UAB, Bellaterra, Spain
[2] CREAF, Campus UAB, Bellaterra, Spain
[3] Institute of Systematic Botany and Ecology, Ulm University, Germany
{debora,aura}@cvc.uab.es

Abstract. Smoothing of biomedical images should preserve gray-level transitions between adjacent tissues, while restoring contours consistent with anatomical structures. Anisotropic diffusion operators are based on image appearance discontinuities (either local or contextual) and might fail at weak inter-tissue transitions. Meanwhile, the output of block-wise and morphological operations is prone to present a block structure due to the shape and size of the considered pixel neighborhood.

In this contribution, we use differential geometry concepts to define a diffusion operator that restricts to image consistent level-sets. In this manner, the final state is a non-uniform intensity image presenting homogeneous inter-tissue transitions along anatomical structures, while smoothing intra-structure texture. Experiments on different types of medical images (magnetic resonance, computerized tomography) illustrate its benefit on a further process (such as segmentation) of images.

Keywords: non-linear smoothing, differential geometry, anatomical structures segmentation, cardiac magnetic resonance, computerized tomography.

1 Introduction

By the sensitivity of medical imaging scanners to tissue physical and chemical properties, the appearance of anatomical structures should be uniform. However, the presence of radiological noise (among other artifacts) disturbs structures homogeneity and suggests an image smoothing before further segmentation of anatomical structures. Medical imaging smoothing should homogenize the intensity inside anatomical structures, while preserving intensity changes at their boundaries without altering their shape. Existing smoothing methods for preserving image features (edges and corners) might be grouped into block-wise and differential operators.

Block-wise operators (like median [1], morphological [1], mean shift [2] or Kuwahara inspired [3]) replace the pixel intensity by a function (usually statistical [2,3]) of neighboring values. Since they can be related to image level-sets

evolution (rather than image intensity evolution) they naturally preserve contrast changes. The counterpart is that evolution of image contours alters their shape. Contours in filtered images deform according to the shape of the structure element defining the pixel neighborhood. In many cases [3,1], even the smoothed image might present a block-wise appearance congruent with the shape of such structure element.

Non-linear anisotropic filtering methods [4, 5, 6] use the formulation of heat diffusion to evolve image intensity. Operators are designed to slow down diffusion across structures and features of interest, which are determined by measures of image appearance discontinuity. Common trends are either the norm of image derivatives (1st order for edges [4] and 2nd order for ridges [6]) or global contextual discontinuities [5]. In order to ensure stability of the diffusion process [7], heat diffuses on the whole image plane, which implies convergence to a uniform intensity image [4,7]. This fact forces adding close-to-data constraints or relying on a given number of iterations (termination problem) to ensure preservation of the image most relevant features [4,8].

In this paper we introduce a differential operator, the Structure-Preserving Diffusion, SPD, which restricts diffusion to a smooth approximation of image contours. Differential geometry arguments [9] ensure stability of the diffusion process. A main contribution is that SPD homogenizes gray-level along regular image contours without altering their shape. In this manner, SPD converges (i.e. the iterative scheme stabilizes) towards a non-uniform image presenting a uniform gray-level inside anatomical structures, while preserving inter tissue transitions.

2   Structure-Preserving Diffusion

Solutions to the heat diffusion equation with initial condition a given image, $I_0(x, y)$, provide a time (scale) dependant family, $I(x, y, t)$, of smoothed versions of $I_0(x, y)$. Heat diffusion is given in divergence form as:

$$I_t(x, y, t) = \operatorname{div}(J\nabla I), \quad I(x, y, 0) = I_0(x, y) \tag{1}$$

where $\nabla I = (I_x, I_y)$ is the image gradient, div is the divergence operator and J is a 2-dimensional symmetric (semi) positive defined tensor that locally describes the way gray level re distributes.

Any symmetric matrix, considered as linear map, diagonalizes [10] in an orthonormal basis:

$$J = Q\Lambda Q^t = \begin{pmatrix} \xi_1 & -\xi_2 \\ \xi_2 & \xi_1 \end{pmatrix} \begin{pmatrix} \lambda_1 & 0 \\ 0 & \lambda_2 \end{pmatrix} \begin{pmatrix} \xi_1 & \xi_1 \\ -\xi_2 & \xi_2 \end{pmatrix}$$

for $\lambda_1 > \lambda_2 >= 0$, J eigenvalues and $\xi = (\xi_1, \xi_2)$ and its perpendicular $\xi^\perp = (-\xi_2, \xi_1)$ J eigenvectors. Symmetric semi-positive defined tensors define a metric in Euclidean space. The unitary vectors associated to the metric are an ellipse with axis of length λ_1, λ_2 oriented along $\xi, \xi^\perp$. The shape of such ellipse describes

the preferred diffusion of heat. In this sense, we can talk about isotropic diffusion (equal eigenvalues) and anisotropic diffusion (distinct and strictly positive eigenvalues). By general theory of partial differential equations [7], equation (1) has a unique solution provided that λ_1, λ_2 do not vanish. However, in such case, $I(x, y, t)$ converges to a constant image [4], so that the diffusion time (iterations in numeric implementations) is a critical issue for restoring an image preserving meaningful structures (termination problem [5]).

In [9], the authors showed that, for null eigenvalues, existence and uniqueness of solutions to (1) is guaranteed as long as the eigenvector of positive eigenvalue defines a differentiable curve. In this case, J represents the projection matrix onto the positive eigenvector and diffusion restricts to its integral curves. It follows that $I(x, y, t)$ converges towards a collection of curves of uniform gray level [9], so that the iterative scheme stabilizes at a non-uniform intensity image. Level-curves of the steady state approximate the original image contours, provided that the positive eigenvector represents their tangent space.

The second moment matrix [11] or structure tensor [12] provides a good description of local image structures. The structure tensor matrix describes the gradient distribution in a local neighborhood of each pixel by averaging the projection matrices onto the image gradient:

$$ST(\rho, \sigma) = g_\rho * \left[\begin{pmatrix} I_x(\sigma) \\ I_y(\sigma) \end{pmatrix} (I_x(\sigma), I_y(\sigma)) \right] = \begin{pmatrix} g_\rho * I_x^2(\sigma) & g_\rho * I_x(\sigma)I_y(\sigma) \\ g_\rho * I_x(\sigma)I_y(\sigma) & g_\rho * I_y^2(\sigma) \end{pmatrix}$$

Image derivatives are computed using gaussian kernels, g_σ, of variance σ (differentiation scale):

$$I_x(\sigma) = g(\sigma)_x * I \text{ and } I_y(\sigma) = g(\sigma)_y * I$$

The projection matrix onto $(I_x(\sigma), I_y(\sigma))$ is averaged using a gaussian of variance ρ (integration scale). Since $ST(\rho, \sigma)$ is the solution to the heat equation with initial condition the projection matrix, its eigenvectors are differentiable (smooth) vector fields that represent image level sets normal (principal eigenvector, ξ) and tangent (secondary eigenvector, $\xi^\perp$) spaces. In the absence of corners (like anatomical contours in bottom right image in fig.1), the vector $\xi^\perp$ is oriented along image consistent contours (in the sense of regular differentiable curves [13]). At textured or noisy regions, $\xi^\perp$ is randomly distributed (upper right image in fig.1).

Our Structure-Preserving Diffusion is given by:

$$I_t = \text{div}(Q\Lambda Q^t \nabla I), \quad I(x, y, 0) = I_0(x, y) \tag{2}$$

with:

$$Q = \left(\xi^\perp, \xi \right) \text{ and } \Lambda = \begin{pmatrix} 1 & 0 \\ 0 & 0 \end{pmatrix}$$

for ξ the principal eigenvector of $ST(\rho, \sigma)$. By $\xi^\perp$ distribution (fig.1), SPD smoothes image gray values along regular structures (bottom right image in fig.1) and performs like a gaussian filter at textured and noisy regions (upper
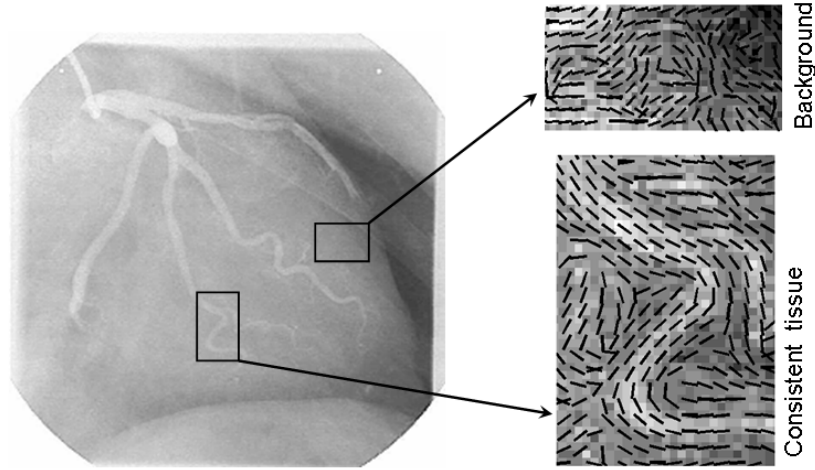
Fig. 1. Vector field representing level curves of an angiography for a vessel (bottom-right image) and a background structure-less area (upper-right image)

right image in fig.1). Its geometric nature makes our restricted diffusion evolution equation converge to a non trivial image that preserves the original image main features as curves of uniform gray level [9]. In this manner, SPD output achieves a uniform response to local image descriptors suitable for a further detection and segmentation of image (anatomical) regions.

3   Results

The goal of our experiments is to show the improvement in quality of SPD images (compared to other filtering approaches) for a further identification of anatomical structures. For the limited length of this communication we have compared SPD to 2 representative techniques: anisotropic and median filtering. SPD has been applied until stabilization of the iterative process, anisotropic diffusion was stopped after 20 iterations and median filter used a 5×5 window. Smoothing techniques have been applied to cardiac Magnetic Resonance (MR) images in short axis (SA) and long axis (LA) views. Image regions segmented using a k-means unsupervised clustering have been compared to manual segmentations in terms of region overlap between two segmentations, X and Y. In particular we have used the Jaccard measure [14] given by $JC := |X \cap Y|/|X \cup Y|$, for $|\cdot|$ the number of pixels.

Fig.2 shows gray-level images and region segmentation with the corresponding manual contours for LA (top rows) and SA (bottom rows) views for, from left to right, non-processed, SPD, Anisotropic Filtering (AF), and Median Filtering (MF). We have segmented three regions: blood (shown in white), myocardial walls (shown in gray) and background (shown in black). Spurious pixels wrongly classified in original views are removed in all filtered images. However, the geometry
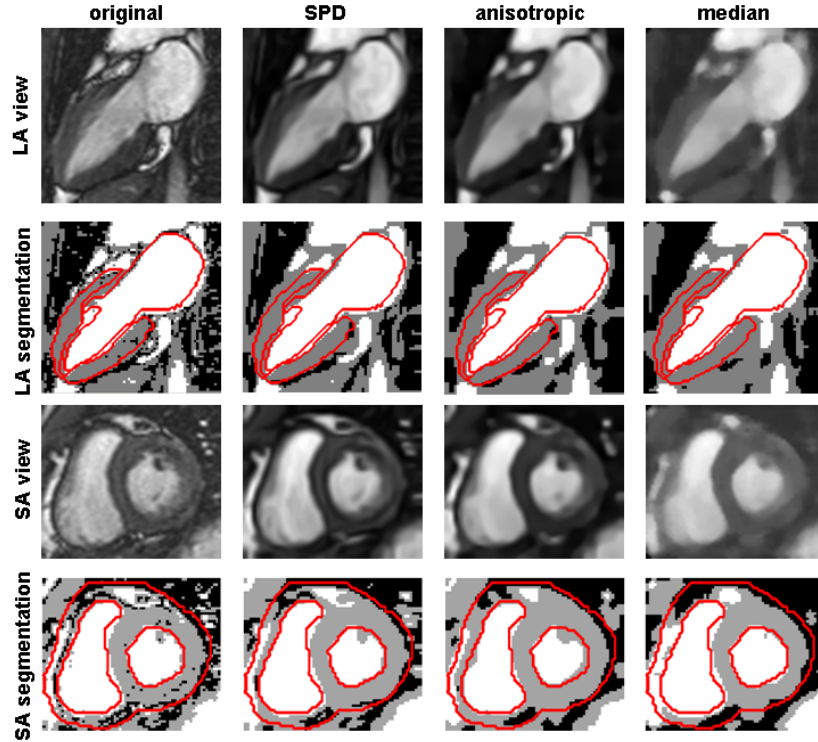
Fig. 2. Performance of smoothing approaches on cardiac magnetic resonance images

Table 1. Jaccard Measure Ranges

	Original		SPD		Anisotropic		Median	
	Blood	Wall	Blood	Wall	Blood	Wall	Blood	Wall
LA	0.7 ± 0.2	0.2 ± 0.3	0.8 ± 0.1	0.5 ± 0.2	0.8 ± 0.1	0.4 ± 0.3	0.8 ± 0.1	0.3 ± 0.3
SA	0.7 ± 0.2	0.5 ± 0.3	0.7 ± 0.2	0.7 ± 0.1	0.7 ± 0.2	0.5 ± 0.3	0.7 ± 0.2	0.5 ± 0.3

of anatomical structures varies across the smoothing type. For LA views the inferior wall of the Left Ventricle (LV) is identified as background in AF images and merged with the adjacent tissue in MF images. Also we observe that the Right Ventricle (RV) blood pool (close to LV inferior wall) merges with LV blood in AF and MF images. SPD images are the only ones preserving the original anatomical structures. Concerning SA views, trabeculae (upper part of LV) and RV wall (left-side of images) are missing in MF images and distorted in AF images. Like in LA views, SPD restores the proper geometry.

Table 1 reports JC statistical ranges for blood and myocardial wall in LA and SA views. For original images blood detection rate is similar in both views, while myocardial wall detection significantly decreases in LA views. For smoothed

images, blood detection is similar for all methods and close to original image ranges. Regarding detection of myocardial walls, median and anisotropic smoothing behave similarly and only improve detections (an increase of JC around 0.12) in the case of LA views. SPD images classification rate is the highest one in both views, increasing the average JC 0.3 in LA views and 0.15 in SA views. It is worth to mention the significant reduction in JC variability for SPD images.

4   Application to Extraction of Plant's Xylem Network

The xylem of plants is a tissue consisting of a tubular network that provides the main pathway for long distance transport of water from roots to leaves [15]. Its properties determine how much water can be transported, as well as, the vulnerability to transport dysfunctions (the formation and propagation of emboli) associated to important stress factors, such as droughts and frost. Recent studies [16] link the topology of the xylem network to its overall transport properties including its vulnerability to the propagation of embolism through the system. Thus, modelling the xylem system for representative plant species would help in developing realistic predictive models of their behavior under extreme drought conditions, a key element to forecast vegetation responses under climate change [17].

The size ($\sim$ microns) and distribution of the conduits, the size of the pores that connect them and the connectivity of the system (i.e., the average number of neighbors per conduit) determine the hydraulic properties of the xylem. X-ray computed micro-tomography (micro-CT) is one of the few imaging techniques allowing high resolution imaging of the 3D xylem network [18]. Left images in fig.3 show a tomographic section of a wooden segment from *Fraxinus americana* and
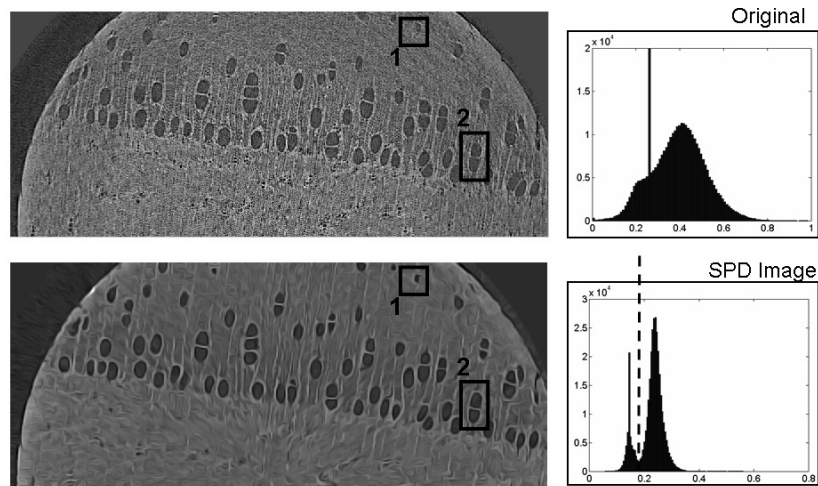

Fig. 3. Benefits of SPD on micro-CT slices of wooden segment: non-processed and SPD images (left) and their intensity histograms (right)
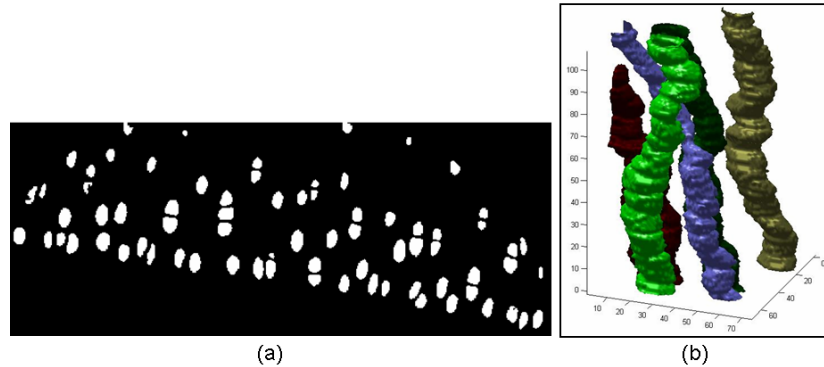
Fig. 4. 3D-Reconstruction of xylem: binary CT-slice, (a) and labelled tubes, (b)

its processed SPD output. Xylem conduits correspond to darker elliptic structures and might appear either isolated or in small (connected) groups separated by a (lighter) thin cell wall. Right plots in fig.3 show gray-level intensity histograms for non-processed (up) and SPD (bottom) images. In the SPD processed image, even the smallest conduits (like the one in square 1) are clearly outlined from the background and there is no loss (i.e. conduit merging) in their connectivity (see the two neighbors in square 2). Furthermore, SPD homogenization of structure intensity produces a bi-modal distribution in histograms separating xylem tubes from background. We have used this property to obtain a detailed 3D reconstruction of the xylem system by simple image processing operators.

Otsu's thresholding method applied to each CT-slice histogram gives the gray-value (vertical dashed line in bottom-right histogram of fig.3) that best separates the two distributions. Morphological operations on binary images are used to remove small structures and close tube holes. Fig.4(a) shows the final binary image representing xylem tubes from SPD image in fig.3. A labelling of the binary 3D block provides the xylem network (as shown in fig.4(b)) and allows the computation of the network connectivity by morphological opening with a structure element of size the maximum separation between connected tubes. These results provide one of the first direct measurements of the connectivity of the xylem network (consistent with previous manual measurements attempts) in any plant species.

5   Discussion and Conclusions

We have presented a diffusion scheme that converges to non-uniform images which present homogenous inter-tissue transitions at consistent anatomical structures and are smooth everywhere else. In order to illustrate independence with respect anatomical shape and medical image modality, we have applied to MR LA and SA views of the heart and to micro-CT of woody segments.

Experiments on MR show that SPD smoothes textured regions similarly to existing methods (blood classification rate in Table 1), while it enhances detection of anatomical contours (myocardial walls statistics in Table 1). A main advantage of SPD is its ability to preserve thin structures (like RV walls in fig.2 or cell walls in fig.4(a)).

Acknowledgments

References

1. Pratt, W.: Digital Image Processing. Wiley, Chichester (1998)
2. Comaniciu, D., Meer, P.: Mean shift analysis and applications. In: Int.Conf. Comp. Vis., ICCV (1999)
3. Papari, G., Petkov, N., Campisi, P.: Artistic edge and corner enhancing smoothing. IEEE Trans. Imag. Proc. 16(10), 2449–2462 (2007)
4. Weickert, J.: A Review of Nonlinear Diffusion Filtering. In: ter Haar Romeny, B.M., Florack, L.M.J., Viergever, M.A. (eds.) Scale-Space 1997. LNCS, vol. 1252, pp. 3–28. Springer, Heidelberg (1997)
5. Chen, K.: Adaptive smoothing via contextual and local discontinuities. IEEE Trans. Pat. Ana. Mach. Intel. 27(10), 1552–1567 (2005)
6. Manniesing, R., Viergever, M., Niessen, W.: Vessel enhancing diffusion a scale space representation of vessel structures. Med. Imag. Ana. 10, 815–825 (2005)
7. Evans, L.: Partial Differential Equations. Berkeley Math. Lect. Notes (1993)
8. Saha, P.K., Udupa, J.: Sacle-based diffusive image filtering preserving boundary sharpness and fine structures. IEEE Trans. Med. Imag. 20, 1140–1155 (2001)
9. Gil, D.: Geometric Differential Operators for Shape Modelling. PhD thesis, Universitat Autonoma de Barcelona (2004)
10. Lang, S.: Linear Algebra. Addison-Wesley, Reading (1971)
11. Mikolajczyk, K., Tuytelaars, T., Schmid, C., et al.: A Comparison of Affine Region Detectors. Int. J. Comp. Vis. 65, 43–72 (2005)
12. Jähne, B.: Spatio-temporal image processing:Theory and Scientific Applications. Springer, Heidelberg (1993)
13. Spivak, M.: A Comprehensive Introduction to Differential Geometry, vol. 1. Publish or Perish, Inc., Houston (1999)
14. Cárdenes, R., Bach, M., Chi, Y., Marras, I., de Luis, R., Anderson, M., Cashman, P., Bultelle, M.: Multimodal evaluation for medical image segmentation. In: Kropatsch, W.G., Kampel, M., Hanbury, A. (eds.) CAIP 2007. LNCS, vol. 4673, pp. 229–236. Springer, Heidelberg (2007)
15. Tyree, M., Zimmermann, M.: Xylem structure and the ascent of sap. Springer, Heidelberg (2002)
16. Loepfe, L., Martinez-Vilalta, J., Piñola, J., et al.: The relevance of xylem network structure for plant hydraulic efficiency and safety. J. Th. Biol. 247, 788–803 (2007)
17. Ciais, P., Reichstein, M., Viovy, N., et al.: Europe-wide reduction in primary productivity caused by the heat and drought in 2003. Nature 437, 529–533 (2005)
18. Trtik, P., Dual, J., Keunecke, D., et al.: 3d imaging of microstructure of spruce wood. J. Struct. Biol. 159, 45–56 (2007)